SIAM J. IMAGING SCIENCES
Vol. 6, No. 3, pp. 1477–1498

© 2013 Society for Industrial and Applied Mathematics

Tracking of a Mobile Target Using Generalized Polarization Tensors*

Habib Ammari†, Thomas Boulier†, Josselin Garnier‡, Hyeonbae Kang§, and Han Wang†

Abstract. In this paper we consider the inverse conductivity problem in two dimensions. We apply an extended Kalman filter to track both the location and the orientation of a small target in motion from multistatic response measurements. We also analyze the effect of the limited-view aspect on the stability and the efficiency of our tracking approach. Our algorithm is based on the use of the generalized polarization tensors, which can be reconstructed from the multistatic response measurements by simply solving a linear system. The reconstruction problem of generalized polarization tensors from multistatic response measurements has the remarkable property that low order generalized polarization tensors are not affected by the error caused by the instability of higher orders in the presence of measurement noise.

Key words. inverse conductivity problem, generalized polarization tensors, target tracking, extended Kalman filter, position and orientation tracking, limited-view data, instability

AMS subject classifications. 35R30, 35B30

DOI. 10.1137/120891022

1. Introduction.

Each domain and conductivity parameter is associated with an infinite number of tensors, called the generalized polarization tensors (GPTs). The concept of GPTs was introduced in [7, 5]. The GPTs contain significant information on the shape of a conductivity inclusion [4, 8, 10]. This occurs in several interesting contexts, particularly low-frequency scattering [17, 5], asymptotic models of dilute composites [25, 11], shape representation and perception [3, 4], invisibility cloaking in the quasi-static regime [9], and potential theory related to certain questions arising in hydrodynamics [26].

Another important use of this concept is for imaging diametrically small conductivity inclusions from multistatic measurements. In multistatic imaging one uses waves to probe for information about an unknown target. These waves can be at zero frequency and consequently modeled by the conductivity equation. They are generated by an array of transmitters and recorded by an array of receivers. Multistatic imaging usually involves two steps. The first step is experimental. It consists in recording the waves generated by sources on an array of receivers. The second step is numerical. It consists in processing the recorded data in order to estimate some relevant features of the unknown conductivity target. Multistatic measurement configuration gives the so-called multistatic response (MSR) matrix, which measures the

*Received by the editors September 11, 2012; accepted for publication (in revised form) May 15, 2013; published electronically August 1, 2013. This work was supported by ERC Advanced Grant Project MULTIMOD–267184 and NRF grants 2009-0090250 and 2010-0017532.
http://www.siam.org/journals/siims/6-3/89102.html

†Department of Mathematics and Applications, École Normale Supérieure, 75005 Paris, France (habib.ammari@ens.fr, boulier@dma.ens.fr, han.wang@ens.fr).

‡Laboratoire de Probabilités et Modèles Aléatoires & Laboratoire Jacques-Louis Lions, Université Paris VII, 75205 Paris Cedex 13, France (garnier@math.jussieu.fr).

§Department of Mathematics, Inha University, Incheon 402-751, Korea (hbkang@inha.ac.kr).

Downloaded 08/02/13 to 147.210.110.133. Redistribution subject to SIAM license or copyright; see http://www.siam.org/journals/ojsa.php

Copyright © by SIAM. Unauthorized reproduction of this article is prohibited.

Downloaded 08/02/13 to 147.210.110.133. Redistribution subject to SIAM license or copyright; see http://www.siam.org/journals/ojsa.php

change in the potential field due to a conductivity target. In fact, if the target is small, then the GPTs are the basic building blocks for the asymptotic expansions of the perturbations of the MSR matrix due to its presence [19, 14, 7]. They can be reconstructed from the MSR matrix by simply solving a linear system. As will be shown later, the reconstruction problem of GPTs from MSR measurements has the remarkable property that low order GPTs are not affected by the error caused by the instability of higher orders in the presence of measurement noise.

Based on small-volume asymptotic expansions, efficient and direct (noniterative) algorithms to determine the location and some geometric features of the inclusions were proposed. We refer the reader to [5, 6] and the references therein for recent developments of this theory. An efficient numerical code for computing the GPTs is described in [13], and a recursive optimization procedure for reconstructing the shape of an inclusion from its GPTs is developed in [10]. On the other hand, it is proved in [4] that high-frequency oscillations of the boundary of an inclusion are contained only in its high-order GPTs. Moreover, by developing a level set version of the recursive optimization scheme developed in [10], it is shown that the GPTs can be used to reconstruct multiple inclusions.

In [2], we have analyzed the stability and the resolving order of GPT as a function of the signal-to-noise ratio in a circular full angle of view setting with coincident sources and receivers. Roughly speaking, the resolving order is the maximum number of GPTs that can be stably reconstructed. We have also developed efficient algorithms for target identification from a dictionary by matching the contracted GPTs (CGPTs). Our dictionary matching technique is based on new invariants for the CGPTs. Explicit relations between the CGPT of scaled, rotated, and translated objects have been established in [2]. The CGPTs are particular linear combinations of the GPTs (called harmonic combinations) and were first introduced in [9].

Our results in [2] strongly suggest that the GPTs can also be used for tracking the location and the orientation of a mobile object. One should have in mind that, in real applications, one would like to localize the target and reconstruct its orientation directly from the MSR data without reconstructing the GPTs. In fact, one can estimate from the MSR measurements the location and the orientation of the target. However, such an algorithm will propagate the error over time, since the noise presented in data is not properly taken into account here. In this paper we develop a CGPT-based tracking algorithm which handles the noise correctly. We apply an extended Kalman filter (EKF) to track both the location and the orientation of a mobile target directly from MSR measurements. For the sake of simplicity, we restrict ourselves to the two dimensional case. The EKF is a generalization of the Kalman filter (KF) to nonlinear dynamical systems. It is robust with respect to noise and computationally inexpensive and therefore is well suited for real-time applications such as tracking [28].

Target tracking is an important task in sonar and radar imaging, security technologies, autonomous vehicle, robotics, and biorobotics; see, for instance, [15, 16, 18, 20, 21, 27]. An example in biorobotics is the weakly electric fish which has the faculty to probe an exterior target with its electric dipole and multiple sensors distributed on the skin [1]. The fish usually swims around the target to acquire information. The use of Kalman-type filtering for target tracking is quite standard; see, for instance, [15, 16, 18, 20, 21, 27].

However, to the best of our knowledge, this is the first time tracking of the orientation of a target is provided. Moreover, we analyze the ill-posed character of both the location and

Copyright © by SIAM. Unauthorized reproduction of this article is prohibited.

Downloaded 08/02/13 to 147.210.110.133. Redistribution subject to SIAM license or copyright; see http://www.siam.org/journals/ojsa.php

orientation tracking in the case of limited-view data. In practice, it is quite realistic to have the sources/receivers cover only a limited angle of view. In this case, the reconstruction of the GPTs becomes more ill-posed than in the full-view case.

It is the aim of this paper to provide a fast algorithm for tracking both the location and the orientation of a mobile target and to precisely analyze the stability of the inverse problem in the limited-view setting.

The paper is organized as follows. In section 2 we recall the conductivity problem and the linear system relating the CGPTs with the MSR data and provide a stability result in the full angle of view setting. In section 3 we present a GPT-based location and orientation tracking algorithm using an EKF and show the numerical results in the full-view setting. In section 4 we analyze the stability of the CGPT reconstruction in the limited-view setting and also test the performance of the tracking algorithm. The paper ends with a few concluding remarks. A brief review of the EKF is given in the appendix.

2. Conductivity problem and reconstruction of CGPTs.

We consider the two-dimensional conductivity problem. Let B be a bounded $\mathcal{C}^2$-domain of characteristic size of order 1 and centered at the origin. Then $D = z + \delta B$ is an inclusion of characteristic size of order δ and centered at z. We denote by $0 < \kappa \neq 1 < +\infty$ its conductivity and

$$\lambda := (\kappa + 1)/(2\kappa - 2) \tag{1}$$

its contrast. In the circular setting, N coincident sources/receivers are evenly spaced on the circle of radius R and centered at the origin O between the angular range $(0, \gamma]$. In the full-view case, $\gamma = 2\pi$, while $\gamma < 2\pi$ in the limited-view configuration. The position of the sth source (and rth receiver) is denoted by x_s (and x_r, respectively) for $s, r = 1, \dots, N$, with $\theta_s = \gamma s/N$ the angular position. We require that the circle be large enough to include the inclusion ($R > \delta$). In the following, we set $\rho := R/\delta > 1$.

2.1. CGPTs and the linear system.

In the presence of D, which is of the form $z + \delta B$, the electrical potential u_s resulting from a source at x_s is given as the solution to the following conductivity problem [2]:

$$\begin{cases} \nabla \cdot ((1 + (\kappa - 1)\chi_D)\nabla u_s)(x) = 0, & x \in \mathbb{R}^2, \\ u_s(x) - \Gamma(x - x_s) = O(|x|^{-1}), & |x| \to +\infty, \end{cases} \tag{2}$$

where $\Gamma(x) = (1/2\pi)\,\log|x|$ is the fundamental solution of the Laplacian in $\mathbb{R}^2$: $\Delta\Gamma(x) = \delta_0(x)$, with δ_0 being the Dirac mass at 0.

We introduce the integral operator $\mathcal{K}_B^* : L^2(\partial B) \to L^2(\partial B)$ as follows: for $\phi \in L^2(\partial B)$

$$\mathcal{K}_B^*[\phi](x) = \int_{\partial B} \frac{\partial \Gamma}{\partial \nu(x)}(x - y)\phi(y)\, d\sigma(y), \quad x \in \partial B,$$

with $\nu(x)$ being the outward normal to ∂B at x. Let the GPT $M_{\alpha\beta}$ for $\alpha, \beta \in \mathbb{N}^2$ be defined by

$$M_{\alpha\beta}(\lambda, B) := \int_{\partial B} (\lambda I - \mathcal{K}_B^*)^{-1} \left(\frac{\partial x^\alpha}{\partial \nu} \right) x^\beta\, d\sigma(x),$$

Copyright © by SIAM. Unauthorized reproduction of this article is prohibited.

Downloaded 08/02/13 to 147.210.110.133. Redistribution subject to SIAM license or copyright; see http://www.siam.org/journals/ojsa.php

where λ is given by (1) and $x^\alpha = x_1^{\alpha_1} x_2^{\alpha_2}$ for $x = (x_1, x_2)$ and $\alpha = (\alpha_1, \alpha_2)$.

Using asymptotic expansion of the fundamental solution Γ, the MSR data $\mathbf{V} = (V_{sr})_{s,r}$, being defined as $V_{sr} = u_s(x_r) - \Gamma(x_r - x_s)$, is linearly related to the GPTs of B as [5, 7]

$$V_{sr} = \sum_{|\alpha|,|\beta|=1}^{K} \frac{\delta^{|\alpha|+|\beta|}}{\alpha!\beta!} \partial^\alpha \Gamma(z - x_s) M_{\alpha\beta}(\lambda, B) \partial^\beta \Gamma(z - x_r) + E_{sr} + W_{sr}, \tag{3}$$

where $\alpha! = \alpha_1!\alpha_2!$ and $\partial^\alpha = \partial_{x_1}^{\alpha_1} \partial_{x_2}^{\alpha_2}$ for $\alpha = (\alpha_1, \alpha_2)$, K denotes the highest order of GPTs in the expansion, $\mathbf{E} = (E_{sr})_{s,r}$ is the truncation error (nonzero if $K < \infty$), and $\mathbf{W} = (W_{sr})_{s,r}$ is the measurement noise independently following the same normal distribution, $W_{sr} \overset{\text{iid}}{\sim} \mathcal{N}(0, \sigma_{\text{noise}}^2)$, of mean zero and variance σ_{noise}^2.

The CGPTs, being defined as a harmonic combination of the GPTs [9], allow us to put (3) into an equivalent form [2],

$$V_{sr} = \sum_{m,n=1}^{K} \underbrace{\frac{1}{2\pi m \rho^m} \left(\cos m\theta_s, \sin m\theta_s\right)}_{\mathbf{A}_{sm}} \underbrace{\begin{pmatrix} \mathbf{M}_{mn}^{cc} & \mathbf{M}_{mn}^{cs} \\ \mathbf{M}_{mn}^{sc} & \mathbf{M}_{mn}^{ss} \end{pmatrix}}_{\mathbf{M}_{mn}} \underbrace{\begin{pmatrix} \cos n\theta_r \\ \sin n\theta_r \end{pmatrix} \frac{1}{2\pi n \rho^n}}_{(\mathbf{A}_{rn})^\top} + E_{sr} + W_{sr}, \tag{4}$$

where $^\top$ denotes the transpose and the CGPT matrix $\mathbf{M} = (\mathbf{M}_{mn})_{m,n}$[1] has dimension $2K \times 2K$.

Note that even though the diagonal terms V_{ss} correspond to have a source and a measurement at the same point in space, they can physically be measured.

Recall that $\mathbf{A} = \mathbf{CD}$, with $\mathbf{C}$ being an $N \times 2K$ matrix constructed from the block $\mathbf{C}_{rm} = (\cos m\theta_r, \sin m\theta_r)$ and $\mathbf{D}$ a $2K \times 2K$ diagonal matrix:

$$\mathbf{C} = \begin{pmatrix} \mathbf{C}_{11} & \mathbf{C}_{12} & \cdots & \mathbf{C}_{1K} \\ \mathbf{C}_{21} & \mathbf{C}_{22} & \cdots & \mathbf{C}_{2K} \\ \cdots & \cdots & \ddots & \cdots \\ \mathbf{C}_{N1} & \mathbf{C}_{N2} & \cdots & \mathbf{C}_{NK} \end{pmatrix}; \quad \mathbf{D} = \frac{1}{2\pi} \begin{pmatrix} \mathbf{I}_2/\rho & & & \\ & \mathbf{I}_2/(2\rho^2) & & \\ & & \ddots & \\ & & & \mathbf{I}_2/(K\rho^K) \end{pmatrix}. \tag{5}$$

Here, $\mathbf{I}_2$ is the 2×2 identity matrix. With this notation in hand, we introduce the linear operator

$$\mathbf{L}(\mathbf{M}) = \mathbf{CDMDC}^\top \tag{6}$$

and rewrite (4) as

$$\mathbf{V} = \mathbf{L}(\mathbf{M}) + \mathbf{E} + \mathbf{W}. \tag{7}$$

In order to reconstruct $\mathbf{M}$, we solve the least-squares problem

$$\min_{\mathbf{M}} \|\mathbf{L}(\mathbf{M}) - \mathbf{V}\|_F^2, \tag{8}$$

[1] Throughout the paper, we will write $\mathbf{M}_{mn}$ for the (m,n)th 2×2 building block, and $(\mathbf{M})_{ab}$ for the (a,b)th entry in $\mathbf{M}$.

Copyright © by SIAM. Unauthorized reproduction of this article is prohibited.

Downloaded 08/02/13 to 147.210.110.133. Redistribution subject to SIAM license or copyright; see http://www.siam.org/journals/ojsa.php

where $\|\cdot\|_F$ denotes the Frobenius norm. Recall that the Frobenius norm of a matrix $\mathbf{A}$ is given by $||\mathbf{A}||_F := \sqrt{\mathrm{tr}(\mathbf{A}\overline{\mathbf{A}}^\top)}$ with tr being the trace.

It is well known that (8) admits a unique minimal norm solution $\mathbf{M}^{\mathrm{est}}$. The linear operator $\mathbf{L}^\dagger$ defined by $\mathbf{M}^{\mathrm{est}} = \mathbf{L}^\dagger(\mathbf{V})$ is called the pseudoinverse of $\mathbf{L}$. The following lemma will be used to explicitly define $\mathbf{L}^\dagger$.

Lemma 2.1. *Let $\mathbf{A}, \mathbf{B}$ be two real matrices of arbitrary dimension, and define the linear operator $\mathbf{L}(\mathbf{X}) = \mathbf{A}\mathbf{X}\mathbf{B}^\top$. If $\mathbf{A}^\dagger, \mathbf{B}^\dagger$ are the pseudoinverses of $\mathbf{A}, \mathbf{B}$, respectively, then the pseudoinverse of $\mathbf{L}$ is given by*

$$\mathbf{L}^\dagger(\mathbf{Y}) = \mathbf{A}^\dagger\mathbf{Y}(\mathbf{B}^\dagger)^\top. \tag{9}$$

Proof. This is a straightforward verification of the definition of the pseudoinverse. Namely, (1) $\mathbf{L}^\dagger\mathbf{L}$ and $\mathbf{L}\mathbf{L}^\dagger$ are self-adjoint; (2) $\mathbf{L}\mathbf{L}^\dagger\mathbf{L} = \mathbf{L}$ and $\mathbf{L}^\dagger\mathbf{L}\mathbf{L}^\dagger = \mathbf{L}^\dagger$. For the first point,

$$\mathbf{L}^\dagger(\mathbf{L}(\mathbf{X})) = \mathbf{A}^\dagger\mathbf{A}\mathbf{X}(\mathbf{B}^\dagger\mathbf{B})^\top,$$

which is self-adjoint since the matrices $\mathbf{A}^\dagger\mathbf{A}$ and $\mathbf{B}^\dagger\mathbf{B}$ are symmetric by the definition of the pseudoinverse; while for the second point, it follows from the definition again that

$$\mathbf{L}(\mathbf{L}^\dagger(\mathbf{L}(\mathbf{X}))) = \mathbf{A}\mathbf{A}^\dagger\mathbf{A}\mathbf{X}(\mathbf{B}\mathbf{B}^\dagger\mathbf{B})^\top = \mathbf{A}\mathbf{X}\mathbf{B}^\top = \mathbf{L}(\mathbf{X}).$$

Similarly, one can verify the self-adjointness of $\mathbf{L}\mathbf{L}^\dagger$ and $\mathbf{L}^\dagger\mathbf{L}\mathbf{L}^\dagger = \mathbf{L}^\dagger$. ∎

2.2. Full-view setting. In [2], we have investigated the resolving order of CGPT reconstruction in the full angle of view setting: $\gamma = 2\pi$. Given $N \geq 2K$, it has been shown that the matrix $\mathbf{C}$ is orthogonal (up to the factor $N/2$),

$$\mathbf{C}^\top\mathbf{C} = \frac{N}{2}\mathbf{I},$$

and the pseudoinverse solution takes the form

$$\mathbf{L}^\dagger(\mathbf{V}) = \frac{4}{N^2}\mathbf{D}^{-1}\mathbf{C}^\top\mathbf{V}\mathbf{C}\mathbf{D}^{-1}. \tag{10}$$

Furthermore, the reconstruction problem is exponentially ill-posed. More precisely, the following result holds.

Proposition 2.2. *Let $\mathbf{e}_{ab}$ be the $2K \times 2K$ matrix whose elements are all zero, except for the element of row a and column b, which is equal to 1. In the circular and full-view setting with $N \geq 2K$, the (a,b)th singular value of the operator $\mathbf{L}$, for $a, b = 1, \ldots, 2K$, is*

$$\lambda_{ab} = N/(8\pi^2\lceil a/2\rceil\lceil b/2\rceil\rho^{\lceil a/2\rceil+\lceil b/2\rceil}), \tag{11}$$

with the matrix $\mathbf{e}_{ab}$ as the right singular vector and $\mathbf{f}_{ab} = \lambda_{ab}^{-1}\mathbf{L}(\mathbf{e}_{ab})$ as the left singular vector. In particular, the condition number of the operator $\mathbf{L}$ is $K^2\rho^{2(K-1)}$.

Proof. Using the fact that $\mathbf{C}^\top\mathbf{C} = \frac{N}{2}\mathbf{I}$, we have, for any square matrices $\mathbf{U}$ and $\mathbf{V}$,

$$\langle \mathbf{L}(\mathbf{U}), \mathbf{L}(\mathbf{V})\rangle = \frac{N^2}{4}\langle \mathbf{D}\mathbf{U}\mathbf{D}, \mathbf{D}\mathbf{V}\mathbf{D}\rangle, \tag{12}$$

Copyright © by SIAM. Unauthorized reproduction of this article is prohibited.

Downloaded 08/02/13 to 147.210.110.133. Redistribution subject to SIAM license or copyright; see http://www.siam.org/journals/ojsa.php

where $\langle \cdot, \cdot \rangle$ is the termwise inner product. Since $\mathbf{D}$ is diagonal and invertible, we conclude that the matrix $\mathbf{e}_{ab}$ is a right singular vector of $\mathbf{L}$ associated to the singular value $\|\mathbf{L}(\mathbf{e}_{ab})\|_F = \|\mathbf{D}\mathbf{e}_{ab}\mathbf{D}\|_F N/2 = N/(8\pi^2 \lceil a/2 \rceil \lceil b/2 \rceil \rho^{\lceil a/2 \rceil + \lceil b/2 \rceil})$. ■

As a simple consequence, we have $\mathbf{L}^\dagger(\mathbf{W})_{ab} = \lambda_{ab}^{-1} \langle \mathbf{W}, f_{ab} \rangle$. When K is sufficiently large, the truncation error $\mathbf{E}$ is $O(\rho^{-K-2})$ and can be neglected if compared to $\mathbf{W}$ [2], and then by the property of white noise

$$\sqrt{\mathbb{E}(((\mathbf{M}^{\text{est}})_{ab} - (\mathbf{M})_{ab})^2)} \lesssim \sqrt{\mathbb{E}((\mathbf{L}^\dagger(\mathbf{W})_{ab}^2))} = \lambda_{ab}^{-1} \sigma_{\text{noise}},$$

which is the result already established in [2]. Hence, it follows from (11) that the reconstruction of high order CGPTs is an ill-posed problem. Nonetheless the system has the remarkable property that low order CGPTs are not affected by the error caused by the instability of higher orders as the following proposition shows.

Proposition 2.3. *Let $\mathbf{M}_K$ denote the CGPTs of order up to K, and let $\mathbf{L}_K$ be the corresponding linear operator in (4). Then, for any order $K_1 \le K_2 < N/2$, the submatrix of $\mathbf{L}_{K_2}^\dagger(\mathbf{V})$ formed by the first $2K_1$ columns and rows is identical to the minimal norm solution $\mathbf{L}_{K_1}^\dagger(\mathbf{V})$.*

Proof. Let the $N \times 2K$ matrix J_K be the row concatenation of the $2K \times 2K$ identity matrix $\mathbf{I}_{2K}$ and a zero matrix. We have $\mathbf{J}_K^\top \mathbf{J}_K = \mathbf{I}_{2K}$, and $\mathbf{J}_{K_1}^\top \mathbf{L}_{K_2}^\dagger(\mathbf{V}) \mathbf{J}_{K_1}$ is the submatrix of $\mathbf{L}_{K_2}^\dagger(\mathbf{V})$ formed by the first $2K_1$ columns and rows. Let $\mathbf{D}_K$ and $\mathbf{C}_K$ be the matrices defined in (5). Because of (10), we have

$$\mathbf{J}_{K_1}^\top \mathbf{L}_{K_2}^\dagger(\mathbf{V}) \mathbf{J}_{K_1} = \frac{4}{N^2} \mathbf{J}_{K_1}^\top \mathbf{D}_{K_2}^{-1} \mathbf{C}_{K_2}^\top \mathbf{V} \mathbf{C}_{K_2} \mathbf{D}_{K_2}^{-1} \mathbf{J}_{K_1}.$$

One can easily see that

$$\mathbf{C}_{K_2} \mathbf{D}_{K_2}^{-1} \mathbf{J}_{K_1} = \mathbf{C}_{K_1} \mathbf{D}_{K_1}^{-1}.$$

Thus, we have

$$\mathbf{J}_{K_1}^\top \mathbf{L}_{K_2}^\dagger(\mathbf{V}) \mathbf{J}_{K_1} = \mathbf{L}_{K_1}^\dagger(\mathbf{V}). \quad ■$$

Numerically, $\mathbf{L}^\dagger$ can be implemented through either the formula (10) or the conjugate gradient (CG) method using (8). Simulations in [2] confirm that in typical situations, say, with $K = 5$ and 10% noise, the reconstructed CGPT is sufficiently accurate for a task such as identification of a target in a dictionary. In the next section we present a location and orientation tracking algorithm for a mobile target based on the concept of CGPTs.

3. Tracking of a mobile target.

In this section, using the relation (7) between the MSR data and the CGPT matrix, we develop an algorithm for tracking both the location and the orientation of the target. It is worth emphasizing that in order to track the location and the orientation of the target, high-order polarization tensors must be used.

At the instant $t \ge 0$, we denote by $z_t = [x_t, y_t]^\top \in \mathbb{R}^2$ the location and by $\theta_t \in [0, 2\pi)$ the orientation of a target D_t.

$$D_t = z_t + R_{\theta_t} D, \tag{13}$$

Copyright © by SIAM. Unauthorized reproduction of this article is prohibited.

Downloaded 08/02/13 to 147.210.110.133. Redistribution subject to SIAM license or copyright; see http://www.siam.org/journals/ojsa.php

where R_{θ_t} is the rotation by θ_t. Let $\mathbf{M}_t$ be the CGPT of D_t and $\mathbf{M}_D$ be the CGPT of D. Then (7) becomes

$$\mathbf{V}_t = \mathbf{L}(\mathbf{M}_t) + \mathbf{E}_t + \mathbf{W}_t, \tag{14}$$

where $\mathbf{E}_t$ is the truncation error and $\mathbf{W}_t$ is the measurement noise at time t. It is worth emphasizing here that the operator $\mathbf{L}$ is independent of t, while the CGPT matrix depends on t.

The objective of *tracking* is to estimate the target's location z_t and orientation θ_t from the MSR data stream $\mathbf{V}_t$. We emphasize that this information is contained in the first two order CGPTs as shown in the previous paper [2]. Precisely, let $\Delta x_t = x_t - x_{t-1}$, $\Delta y_t = y_t - y_{t-1}$, and $\Delta\theta_t = \theta_t - \theta_{t-1}$; then the following relations (when they are well defined) exist between the CGPT of D_t and D_{t-1} [2]:

$$\begin{aligned}
\mathbf{N}^{(1)}_{12}(D_t)/\mathbf{N}^{(1)}_{11}(D_t) &= 2(\Delta x_t + i\Delta y_t) + e^{i\Delta\theta_t}\mathbf{N}^{(1)}_{12}(D_{t-1})/\mathbf{N}^{(1)}_{11}(D_{t-1}),\\
\mathbf{N}^{(2)}_{12}(D_t)/\mathbf{N}^{(2)}_{11}(D_t) &= 2(\Delta x_t + i\Delta y_t) + e^{i\Delta\theta_t}\mathbf{N}^{(2)}_{12}(D_{t-1})/\mathbf{N}^{(2)}_{11}(D_{t-1}).
\end{aligned} \tag{15}$$

Hence when the linear system (15) is solvable, one can estimate z_t, θ_t by solving and accumulating $\Delta x_t, \Delta y_t$, and $\Delta\theta_t$. However, such an algorithm will propagate the error over time, since the noise presented in data is not properly taken into account here.

In the following we develop a CGPT-based tracking algorithm using the EKF, which correctly handles the noise. We recall first the definition of complex CGPT, with which a simple relation between $\mathbf{M}_t$ and $\mathbf{M}_D$ can be established.

3.1. Time relationship between CGPTs.

Let $u = (1, i)^\top$. The complex CGPTs $\mathbf{N}^{(1)}, \mathbf{N}^{(2)}$ are defined by

$$\begin{aligned}
\mathbf{N}^{(1)}_{mn} &= (\mathbf{M}^{cc}_{mn} - \mathbf{M}^{ss}_{mn}) + i(\mathbf{M}^{cs}_{mn} + \mathbf{M}^{sc}_{mn}) = u^\top \mathbf{M}_{mn} u,\\
\mathbf{N}^{(2)}_{mn} &= (\mathbf{M}^{cc}_{mn} + \mathbf{M}^{ss}_{mn}) + i(\mathbf{M}^{cs}_{mn} - \mathbf{M}^{sc}_{mn}) = u^H \mathbf{M}_{mn} u,
\end{aligned}$$

where H denotes the Hermitian transpose. Therefore, we have

$$\mathbf{N}^{(1)} = \mathbf{U}^\top \mathbf{M}\mathbf{U} \quad \text{and} \quad \mathbf{N}^{(2)} = \mathbf{U}^H \mathbf{M}\mathbf{U}, \tag{16}$$

where the matrix $\mathbf{U}$ of dimension $2K \times K$ over the complex fields is defined by

$$\mathbf{U} = \begin{pmatrix} u & 0 & \dots & 0 \\ 0 & u & \dots & 0 \\ \vdots & & \ddots & \vdots \\ 0 & \dots & 0 & u \end{pmatrix}. \tag{17}$$

It is worth mentioning that $\mathbf{N}^{(1)}$ and $\mathbf{N}^{(2)}$ are complex matrices of dimension $K \times K$.

To recover the CGPT $\mathbf{M}_{mn}$ from the complex CGPTs $\mathbf{N}^{(1)}, \mathbf{N}^{(2)}$, we simply use the relations

$$\begin{aligned}
\mathbf{M}^{cc}_{mn} &= \frac{1}{2}\Re(\mathbf{N}^{(1)}_{mn} + \mathbf{N}^{(2)}_{mn}),\ \mathbf{M}^{cs}_{mn} = \frac{1}{2}\Im(\mathbf{N}^{(1)}_{mn} + \mathbf{N}^{(2)}_{mn}),\\
\mathbf{M}^{sc}_{mn} &= \frac{1}{2}\Im(\mathbf{N}^{(1)}_{mn} - \mathbf{N}^{(2)}_{mn}),\ \mathbf{M}^{ss}_{mn} = \frac{1}{2}\Re(\mathbf{N}^{(2)}_{mn} - \mathbf{N}^{(1)}_{mn}),
\end{aligned} \tag{18}$$

Copyright © by SIAM. Unauthorized reproduction of this article is prohibited.

Downloaded 08/02/13 to 147.210.110.133. Redistribution subject to SIAM license or copyright; see http://www.siam.org/journals/ojsa.php

where $\Re, \Im$ are the real and imaginary parts of a complex number, respectively. For two targets D_t, D satisfying (13), the following relationships between their complex CGPT hold [2]:

$$\mathbf{N}^{(1)}(D_t) = \mathbf{F}_t^\top \mathbf{N}^{(1)}(D)\mathbf{F}_t, \tag{19a}$$

$$\mathbf{N}^{(2)}(D_t) = \mathbf{F}_t^H \mathbf{N}^{(2)}(D)\mathbf{F}_t, \tag{19b}$$

where $\mathbf{F}_t$ is a upper triangle matrix with the (m,n)th entry given by

$$(\mathbf{F}_t)_{mn} = \binom{n}{m}(x_t + iy_t)^{n-m}e^{im\theta_t}. \tag{20}$$

Linear operator $\mathbf{T}_t$. Now one can explicitly find a linear operator $\mathbf{T}_t$ (the underlying scalar field is $\mathbb{R}$) which depends only on z_t, θ_t, such that $\mathbf{M}_t = \mathbf{T}_t(\mathbf{M}_D)$, and (14) becomes

$$\mathbf{V}_t = \mathbf{L}(\mathbf{T}_t(\mathbf{M}_D)) + \mathbf{E}_t + \mathbf{W}_t. \tag{21}$$

For doing so, we set $\mathbf{J}_t := \mathbf{U}\mathbf{F}_t$, where $\mathbf{U}$ is given by (17). Then, a straightforward computation using (16), (18), and (19) shows that

$$\begin{aligned} \mathbf{M}^{cc}(D_t) &= \Re\mathbf{J}_t^\top \mathbf{M}_D \Re\mathbf{J}_t,\ \ \mathbf{M}^{cs}(D_t) = \Re\mathbf{J}_t^\top \mathbf{M}_D \Im\mathbf{J}_t, \\ \mathbf{M}^{sc}(D_t) &= \Im\mathbf{J}_t^\top \mathbf{M}_D \Re\mathbf{J}_t,\ \ \mathbf{M}^{ss}(D_t) = \Im\mathbf{J}_t^\top \mathbf{M}_D \Im\mathbf{J}_t, \end{aligned} \tag{22}$$

where $\mathbf{M}^{cc}(D_t), \mathbf{M}^{cs}(D_t), \mathbf{M}^{sc}(D_t), \mathbf{M}^{ss}(D_t)$ are defined in (4). Therefore, we get the operator $\mathbf{T}_t$:

$$\begin{aligned} \mathbf{T}_t(\mathbf{M}_D) = {} & \Re\mathbf{U}(\Re\mathbf{J}_t^\top \mathbf{M}_D \Re\mathbf{J}_t)\Re\mathbf{U}^\top + \Re\mathbf{U}(\Re\mathbf{J}_t^\top \mathbf{M}_D \Im\mathbf{J}_t)\Im\mathbf{U}^\top \\ & + \Im\mathbf{U}(\Im\mathbf{J}_t^\top \mathbf{M}_D \Re\mathbf{J}_t)\Re\mathbf{U}^\top + \Im\mathbf{U}(\Im\mathbf{J}_t^\top \mathbf{M}_D \Im\mathbf{J}_t)\Im\mathbf{U}^\top = \mathbf{M}_t. \end{aligned} \tag{23}$$

3.2. Tracking by the EKF. The EKF is a generalization of the KF to nonlinear dynamical systems. Unlike the KF, which is an optimal estimator for linear systems with Gaussian noise, the EKF is no longer optimal, but it remains robust with respect to noise and computationally inexpensive and therefore is well suited for real-time applications such as tracking. We establish here the *system state* and the *observation* equations which are fundamental to the EKF and refer readers to Appendix B for its algorithmic details.

3.2.1. System state observation equations. We assume that the position of the target is subjected to an external driving acceleration that has the form of a white noise. In other words, the velocity $(V(\tau))_{\tau\in\mathbb{R}^+}$ of the target is given in terms of a two-dimensional Brownian motion $(W_a(\tau))_{\tau\in\mathbb{R}^+}$, and its position $(Z(\tau))_{\tau\in\mathbb{R}^+}$ is given in terms of the integral of this Brownian motion:

$$V(\tau) = V_0 + \sigma_a W_a(\tau), \qquad Z(\tau) = Z_0 + \int_0^\tau V(s)ds.$$

Here, $V_0 = V(0)$ is a constant vector. The orientation $(\Theta(\tau))_{\tau\in\mathbb{R}^+}$ of the target is subjected to random fluctuations, and its angular velocity is given in terms of an independent white noise, so that the orientation is given in terms of a one-dimensional Brownian motion $(W_\theta(\tau))_{\tau\in\mathbb{R}^+}$:

$$\Theta(\tau) = \Theta_0 + \sigma_\theta W_\theta(\tau).$$

Copyright © by SIAM. Unauthorized reproduction of this article is prohibited.

Downloaded 08/02/13 to 147.210.110.133. Redistribution subject to SIAM license or copyright; see http://www.siam.org/journals/ojsa.php

We observe the target at discrete times $t\Delta\tau$, $t \in \mathbb{N}$, with time step $\Delta\tau$. We denote $z_t = Z(t\Delta\tau)$, $v_t = V(t\Delta\tau)$, and $\theta_t = \Theta(t\Delta\tau)$. They obey the recursive relations

$$\begin{aligned} v_t &= v_{t-1} + a_t, & a_t &= \sigma_a\big(W_a(t\Delta\tau) - W_a((t-1)\Delta\tau)\big), \\ z_t &= z_{t-1} + v_{t-1}\Delta\tau + b_t, & b_t &= \sigma_a \int_{(t-1)\Delta\tau}^{t\Delta\tau} W_a(s) - W_a((t-1)\Delta\tau)ds, \\ \theta_t &= \theta_{t-1} + c_t, & c_t &= \sigma_\theta\big(W_\theta(t\Delta\tau) - W_\theta((t-1)\Delta\tau)\big). \end{aligned} \tag{24}$$

Since the increments of the Brownian motions are independent of each other, the vectors $(U_t)_{t\geq 1}$ given by

$$U_t = \begin{pmatrix} a_t \\ b_t \\ c_t \end{pmatrix}$$

are independent and identically distributed with the multivariate normal distribution with mean zero and covariance matrix $\mathbf{\Sigma}$ given by

$$\mathbf{\Sigma} = \Delta\tau \begin{pmatrix} \sigma_a^2\mathbf{I}_2 & \frac{\sigma_a^2}{2}\Delta\tau\mathbf{I}_2 & 0 \\ \frac{\sigma_a^2}{2}\Delta\tau\mathbf{I}_2 & \frac{\sigma_a^2}{3}\Delta\tau^2\mathbf{I}_2 & 0 \\ 0 & 0 & \sigma_\theta^2 \end{pmatrix}. \tag{25}$$

The evolution of the state vector

$$X_t = \begin{pmatrix} v_t \\ z_t \\ \theta_t \end{pmatrix}$$

takes the form

$$X_t = \mathbf{F}X_{t-1} + U_t, \qquad \mathbf{F} = \begin{pmatrix} \mathbf{I}_2 & 0 & 0 \\ \Delta\tau\mathbf{I}_2 & \mathbf{I}_2 & 0 \\ 0 & 0 & 1 \end{pmatrix}. \tag{26}$$

The observation made at time t is the MSR matrix $\mathbf{V}_t$ given by (21), where the system state X_t is implicitly included in the operator $\mathbf{T}_t$. We suppose that the truncation error $\mathbf{E}_t$ is small compared to the measurement noise so that it can be dropped in (21), and that the Gaussian white noise $\mathbf{W}_t$'s of different times are mutually independent. We emphasize that the velocity vector v_t of the target does not contribute to (21), which can be seen from (13). To highlight the dependence upon z_t, θ_t, we introduce a function $\mathbf{h}$ which is nonlinear in z_t, θ_t and takes $\mathbf{M}_D$ as a parameter, such that

$$\mathbf{h}(X_t; \mathbf{M}_D) = \mathbf{h}(z_t, \theta_t; \mathbf{M}_D) = \mathbf{L}(\mathbf{T}_t(\mathbf{M}_D)). \tag{27}$$

Then together with (26) we get the following *system state* and *observation* equations:

$$X_t = \mathbf{F}X_{t-1} + U_t, \tag{28a}$$

$$\mathbf{V}_t = \mathbf{h}(X_t; \mathbf{M}_D) + \mathbf{W}_t. \tag{28b}$$

Note that (28a) is linear, so in order to apply the EKF on (28), we need only linearize (28b) or, in other words, calculate the partial derivatives of $\mathbf{h}$ with respect to x_t, y_t, θ_t.

Copyright © by SIAM. Unauthorized reproduction of this article is prohibited.

Downloaded 08/02/13 to 147.210.110.133. Redistribution subject to SIAM license or copyright; see http://www.siam.org/journals/ojsa.php

3.2.2. Linearization of the observation equation. Clearly, the operator $\mathbf{L}$ contains only the information concerning the acquisition system and does not depend on x_t, y_t, θ_t. So by (27), we have

$$\partial_{x_t}\mathbf{h} = \mathbf{L}(\partial_{x_t}\mathbf{T}_t(\mathbf{M}_D)), \tag{29}$$

while the calculation for $\partial_{x_t}\mathbf{T}_t$ is straightforward using (23). We have

$$\begin{aligned}\partial_{x_t}\mathbf{T}_t(\mathbf{M}_D) &= \Re\mathbf{U}\partial_{x_t}(\Re\mathbf{J}_t^\top\mathbf{M}_D\Re\mathbf{J}_t)\Re\mathbf{U}^\top + \Re\mathbf{U}\partial_{x_t}(\Re\mathbf{J}_t^\top\mathbf{M}_D\Im\mathbf{J}_t)\Im\mathbf{U}^\top \\ &\quad + \Im\mathbf{U}\partial_{x_t}(\Im\mathbf{J}_t^\top\mathbf{M}_D\Re\mathbf{J}_t)\Re\mathbf{U}^\top + \Im\mathbf{U}\partial_{x_t}(\Im\mathbf{J}_t^\top\mathbf{M}_D\Im\mathbf{J}_t)\Im\mathbf{U}^\top,\end{aligned} \tag{30}$$

where the derivatives are given by

$$\begin{aligned}\partial_{x_t}(\Re\mathbf{J}_t^\top\mathbf{M}_D\Re\mathbf{J}_t) &= \Re(\partial_{x_t}\mathbf{J}_t^\top)\mathbf{M}_D\Re\mathbf{J}_t + \Re\mathbf{J}_t^\top\mathbf{M}_D\Re(\partial_{x_t}\mathbf{J}_t),\\
\partial_{x_t}(\Re\mathbf{J}_t^\top\mathbf{M}_D\Im\mathbf{J}_t) &= \Re(\partial_{x_t}\mathbf{J}_t^\top)\mathbf{M}_D\Im\mathbf{J}_t + \Re\mathbf{J}_t^\top\mathbf{M}_D\Im(\partial_{x_t}\mathbf{J}_t),\\
\partial_{x_t}(\Im\mathbf{J}_t^\top\mathbf{M}_D\Re\mathbf{J}_t) &= \Im(\partial_{x_t}\mathbf{J}_t^\top)\mathbf{M}_D\Re\mathbf{J}_t + \Im\mathbf{J}_t^\top\mathbf{M}_D\Re(\partial_{x_t}\mathbf{J}_t),\\
\partial_{x_t}(\Im\mathbf{J}_t^\top\mathbf{M}_D\Im\mathbf{J}_t) &= \Im(\partial_{x_t}\mathbf{J}_t^\top)\mathbf{M}_D\Im\mathbf{J}_t + \Im\mathbf{J}_t^\top\mathbf{M}_D\Im(\partial_{x_t}\mathbf{J}_t),\end{aligned}$$

and $\partial_{x_t}\mathbf{J}_t = \mathbf{U}\partial_{x_t}\mathbf{F}_t$. The (m,n)th entry of the matrix $\partial_{x_t}\mathbf{F}_t$ is given by

$$(\partial_{x_t}\mathbf{F}_t)_{m,n} = \binom{n}{m}(n-m)z_t^{n-m-1}e^{im\theta_t}. \tag{31}$$

The derivatives $\partial_{y_t}\mathbf{T}_t(\mathbf{M}_D)$ and $\partial_{\theta_t}\mathbf{T}_t(\mathbf{M}_D)$ are calculated in the same way.

3.3. Numerical experiments of tracking in the full-view setting. Here we show the performance of the EKF in a full angle of view setting with the shape "A" as target D, which has diameter 10 and is centered at the origin. The path (z_t, θ_t) is simulated according to the model (24) during a period of 10 seconds ($\Delta\tau = 0.01$ second), with parameters $\sigma_a = 2, \sigma_\theta = 0.5$ and the initial state $X_0 = (v_0, z_0, \theta_0)^\top = (-1, 1, 5, -5, 3\pi/2)^\top$. We make sure that the target is always included inside the measurement circle on which $N = 20$ sources/receivers are fixed; see Figure 1. The data stream $\mathbf{V}_t$ is generated by first calculating the MSR matrix corresponding to each $D_t, t \geq 0$, and then adding a white noise.

Suppose that the CGPT of D is correctly determined (for instance, by identifying the target in a dictionary [2]). Then we use the first two orders CGPT $\mathbf{M}_D$ of D in (28b), and take $(0, 0, 10, -0.5, 0)^\top$ as the initial guess of X_0 for the EKF.

We add 10% and 20% of noise to data and show the results of tracking in Figures 2 (a), (c), and (e). We see that the EKF can find the true system state, despite the poor initial guess, and the tracking precision decays as the measurement noise level gets higher. The same experiment with a small target (of the same shape) of diameter 1 is repeated in Figures 2 (b), (d), and (f), where the tracking of the position remains correct, and on the contrary, that of the orientation fails when the noise level is high. Such a result is in accordance with physical intuitions. In fact, the position of a small target can be easily localized in the far field, while its orientation can be correctly determined only in the near field. Moreover, if we compare Figures 2 (e) and (f), then we can see that the smaller the target is, the more sensitive to noise the angle tracking is.

Copyright © by SIAM. Unauthorized reproduction of this article is prohibited.

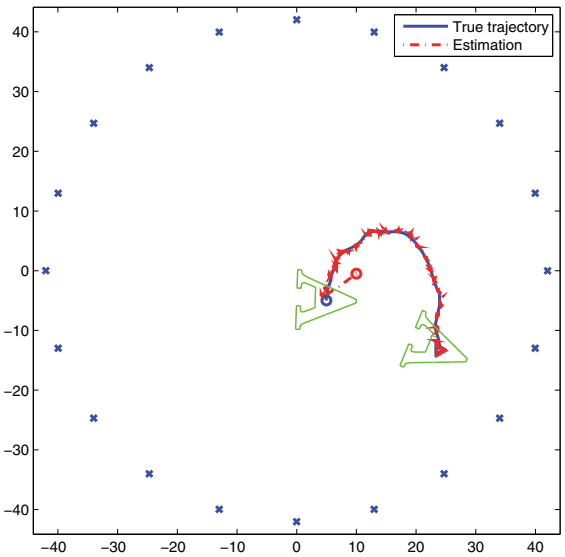

Figure 1. *Trajectory of the letter "A" and the estimation by EKF. The initial position is* $(5, -5)$*, while the initial guess given to EKF is* $(10, -0.5)$*. The crosses indicate the position of sources/receivers, while the circle and the triangle indicate the starting and the final positions of the target, respectively. In blue is the true trajectory and in red the estimated one.*

4. CGPT reconstruction and tracking problem in the limited-view setting.

In this section we study the stability of the CGPT reconstruction and tracking problem in the case where $0 < \gamma < 2\pi$, always under the condition that $N > 2K$, i.e., the number of sources/receivers is two times larger than the highest order of CGPTs to be reconstructed. Unlike in the full-view case, the matrix $\mathbf{C}$ defined by (5) is no longer orthogonal in general; nonetheless one can still establish the SVD of $\mathbf{L}$ similarly as in Proposition 2.2.

Proposition 4.1. *Consider the concentric and limited-view setting with* $N \geq 2K$*, and suppose that* $\mathbf{C}$ *is of maximal rank. Let* $\{\mu_n\}$ *be the* n*th largest eigenvalue of the matrix* $\mathbf{DC}^\top\mathbf{CD}$*, and let* $\{v_n\}$ *be the associated orthonormal eigenvector. Then the* (a, b)*th singular value of the operator* $\mathbf{L}$ *is* $\lambda_{ab} = \sqrt{\mu_a \mu_b}$*, with the associated left singular vector the matrix* $\mathbf{g}_{ab} = v_a v_b^\top$*. In particular, the condition number of the operator* $\mathbf{L}$ *is*

$$\operatorname{cond}(\mathbf{L}) = \operatorname{cond}(\mathbf{DC}^\top\mathbf{CD}) \leq \operatorname{cond}(\mathbf{C})^2 K^2 \rho^{2(K-1)}, \tag{32}$$

with $\operatorname{cond}(\mathbf{C})$ *being the condition number of the matrix* $\mathbf{C}$*.*

Proof. We first note that for any matrices $\mathbf{U}, \mathbf{V}$ we have

$$\langle \mathbf{L}(\mathbf{U}), \mathbf{L}(\mathbf{V}) \rangle = \langle \mathbf{U}, (\mathbf{DC}^\top\mathbf{CD})\mathbf{V}(\mathbf{DC}^\top\mathbf{CD}) \rangle.$$

Taking $\mathbf{g}_{ab} = v_a v_b^\top$ and $\mathbf{g}_{a'b'} = v_{a'} v_{b'}^\top$, we get

$$\begin{aligned} \langle \mathbf{L}(\mathbf{g}_{ab}), \mathbf{L}(\mathbf{g}_{a'b'}) \rangle &= \mu_{a'} \langle v_a v_b^\top, v_{a'} v_{b'}^\top (\mathbf{DC}^\top\mathbf{CD}) \rangle = \mu_{a'}\mu_{b'} \langle v_a v_b^\top, v_{a'} v_{b'}^\top \rangle \\ &= \delta_{aa'}\delta_{bb'}\mu_a\mu_b, \end{aligned}$$

Downloaded 08/02/13 to 147.210.110.133. Redistribution subject to SIAM license or copyright; see http://www.siam.org/journals/ojsa.php

Copyright © by SIAM. Unauthorized reproduction of this article is prohibited.

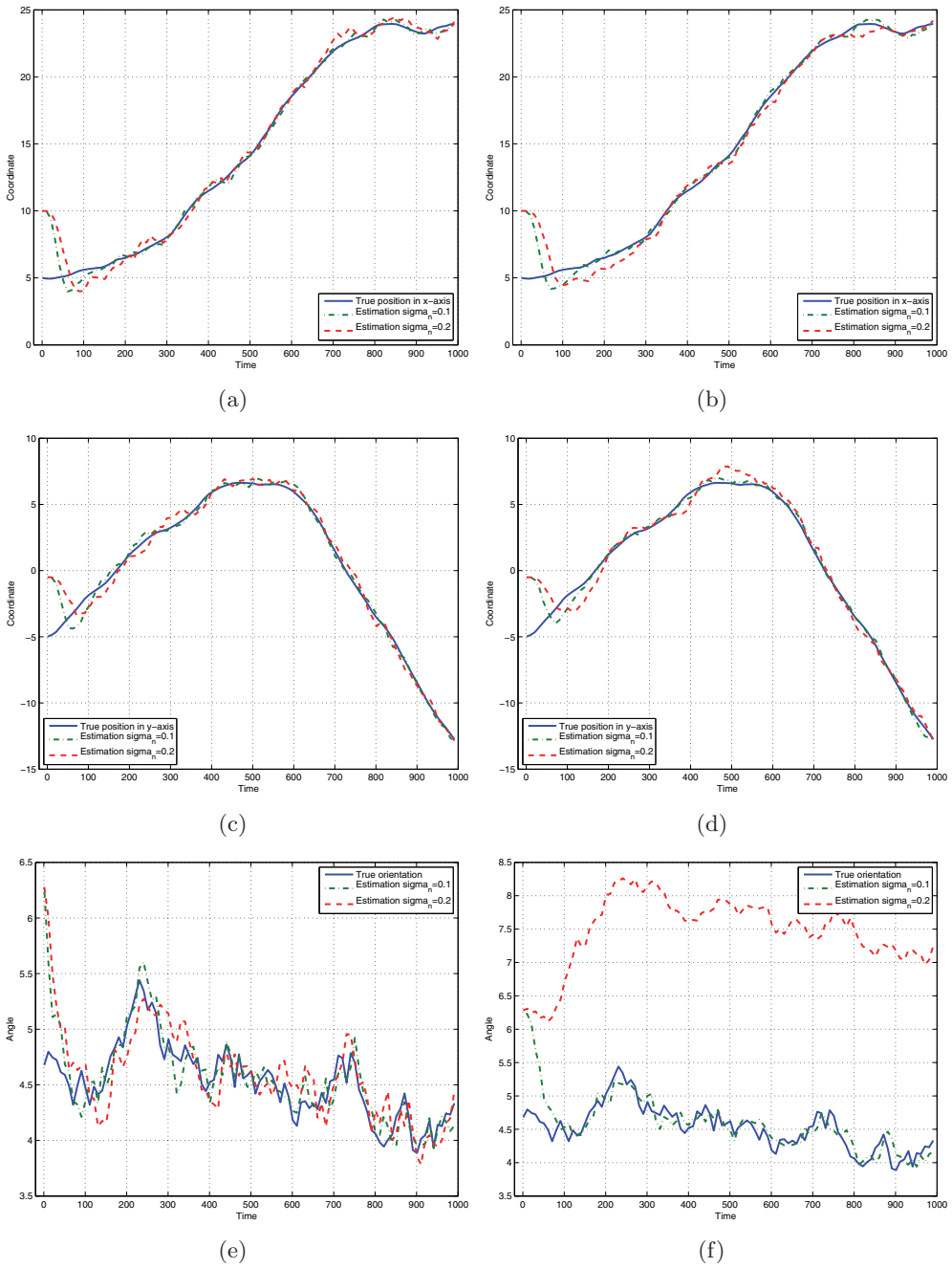

Figure 2. *Results of tracking using the configuration of Figure 1 at different noise levels. First row: Coordinate in x-axis. Second row: Coordinate in y-axis. Last row: Orientation. In the first column the target has size 10, while in the second column the target has size 1. The solid line always indicates the true system state.*

Downloaded 08/02/13 to 147.210.110.133. Redistribution subject to SIAM license or copyright; see http://www.siam.org/journals/ojsa.php

Copyright © by SIAM. Unauthorized reproduction of this article is prohibited.

Downloaded 08/02/13 to 147.210.110.133. Redistribution subject to SIAM license or copyright; see http://www.siam.org/journals/ojsa.php

where $\delta_{aa'}$ is the Kronecker symbol, which implies that $\|\mathbf{L}(\mathbf{g}_{ab})\|_F = \sqrt{\mu_a \mu_b}$ is the (a,b)th singular value of $\mathbf{L}$. If we denote by $\rho_{\max}(\cdot)$ and $\rho_{\min}(\cdot)$ the maximal and minimal singular values of a matrix, then

$$\rho_{\max}(\mathbf{D}\mathbf{C}^\top\mathbf{C}\mathbf{D}) = \rho_{\max}(\mathbf{C}\mathbf{D})^2 \le \rho_{\max}(\mathbf{C})^2\rho_{\max}(\mathbf{D})^2,$$
$$\rho_{\min}(\mathbf{D}\mathbf{C}^\top\mathbf{C}\mathbf{D}) = \rho_{\min}(\mathbf{C}\mathbf{D})^2 \ge \rho_{\min}(\mathbf{C})^2\rho_{\min}(\mathbf{D})^2,$$

and the condition number of $\mathbf{L}$ is therefore bounded by $\mathrm{cond}(\mathbf{C})^2K^2\rho^{2(K-1)}$. ■

4.1. Injectivity of C. We denote by V_K the vector space of functions of the form

$$f(\theta) = \sum_{k=-K}^{K} c_k e^{ik\theta}, \tag{33}$$

with $c_k \in \mathbb{C}$, and by V_K^0 the subspace of V_K such that $c_0 = 0$. Functions of V_K^0 can be written as

$$f(\theta) = \sum_{k=1}^{K} \alpha_k \cos(k\theta) + \beta_k \sin(k\theta), \tag{34}$$

with $\alpha_k, \beta_k \in \mathbb{C}$. Observe that taking discrete samples of (34) at $\theta_s = \gamma s/N$ is nothing but applying the matrix $\mathbf{C}$ on a coefficient vector $(\alpha_1, \beta_1, \ldots, \alpha_K, \beta_K)$. We have the following result.

Proposition 4.2. *For any $N \ge 2K$, the matrix $\mathbf{C}$ is of maximal rank.*

Proof. Multiplying $f \in V_K^0$ in (33) by $e^{iK\theta}$ and using the fact that $c_0 = 0$, we have

$$\begin{aligned} e^{iK\theta}f(\theta) &= \sum_{k=0}^{K-1} c_{k-K}e^{ik\theta} + \sum_{k=K+1}^{2K} c_{k-K}e^{ik\theta} \\ &= \sum_{k=0}^{K-1} c_{k-K}e^{ik\theta} + \sum_{k=K}^{2K-1} e^{i\theta}c_{k+1-K}e^{ik\theta} = \sum_{k=0}^{2K-1} \tilde{c}_k e^{ik\theta}, \end{aligned} \tag{35}$$

where $\tilde{c}_k = c_{k-K}$ for $k = 0, \ldots, K-1$ and $\tilde{c}_k = e^{i\theta}c_{k+1-K}$ for $k = K, \ldots, 2K-1$. The N vectors $v_s := (e^{ik\theta_s})_{k=0,\ldots,2K-1}$ are linearly independent since they are the first $2K \le N$ rows of an $N \times N$ Vandermonde matrix. Therefore, $f(\theta_s) = 0$ for $s = 1, \ldots, N$ implies that $\tilde{c}_k = 0$ for all $k = 0, \ldots, 2K-1$, which means that $\mathbf{C}$ is of maximal rank. ■

Consequently, for an arbitrary range $0 < \gamma \le 2\pi$, a sufficient condition to uniquely determine the CGPTs of order up to K is to have $N \ge 2K$ sources/receivers.

4.2. Explicit left inverse of C. We denote by $D_K(\theta)$ the Dirichlet kernel of order K:

$$D_K(\theta) = \sum_{k=-K}^{K} e^{ik\theta} = \frac{\sin((K+1/2)\theta)}{\sin(\theta/2)}. \tag{36}$$

We state without proof the following well-known result about V_K.

Copyright © by SIAM. Unauthorized reproduction of this article is prohibited.

Downloaded 08/02/13 to 147.210.110.133. Redistribution subject to SIAM license or copyright; see http://www.siam.org/journals/ojsa.php

Lemma 4.3. *The function* $\{D_K(\theta - \frac{2\pi n}{2K+1})\}_{n=0,\dots,2K}$ *is an orthogonal basis of* V_K. *For any* $f, g \in V_K$, *the following identity holds:*

$$\frac{1}{2\pi}\int_0^{2\pi} f(\theta)g^*(\theta)d\theta = \frac{1}{2K+1}\sum_{n=1}^{2K+1} f\left(\frac{2\pi n}{2K+1}\right) g\left(\frac{2\pi n}{2K+1}\right), \tag{37}$$

where * *denotes the complex conjugate. In particular, we have for* $n = 0, \dots, 2K$

$$\frac{1}{2\pi}\int_0^{2\pi} f(\theta)D_K\left(\theta - \frac{2\pi n}{2K+1}\right)d\theta = f\left(\frac{2\pi n}{2K+1}\right). \tag{38}$$

Lemma 4.4. *Given a set of* $N > 2K$ *different points* $0 < \theta_1 < \cdots < \theta_N \le 2\pi$, *there exist interpolation kernels* $h_s \in V_{\lfloor N/2 \rfloor}$ *for* $s = 1, \dots, N$ *such that*

$$f(\theta) = \sum_{s=1}^{N} f(\theta_s)h_s(\theta) \text{ for any } f \in V_K. \tag{39}$$

Proof. When the number of points N is odd, it is well known [29] that h_s takes the form

$$h_s(\theta) = \prod_{t=1, t\neq s}^{N} \frac{\sin\left(\frac{\theta-\theta_t}{2}\right)}{\sin\left(\frac{\theta_s-\theta_t}{2}\right)}. \tag{40}$$

When N is even, by a result established in [24]

$$h_s(\theta) = \cos\left(\frac{\theta-\theta_s}{2}\right)\prod_{t=1, t\neq s}^{N} \frac{\sin\left(\frac{\theta-\theta_t}{2}\right)}{\sin\left(\frac{\theta_s-\theta_t}{2}\right)}. \tag{41}$$

It is easy to see that in both cases h_s belongs to $V_{\lfloor N/2 \rfloor}$. ∎

Now we can explicitly find a left inverse for $\mathbf{C}$.

Proposition 4.5. *Under the same condition as in Lemma 4.4, we denote by* h_s *the interpolation kernel and define the matrix* $\tilde{\mathbf{C}} = (\tilde{\mathbf{C}}_{ks})_{k,s}$ *as*

$$\tilde{\mathbf{C}}_{2k-1,s} = \frac{1}{\pi}\int_0^{2\pi} h_s(\theta)\cos(k\theta)d\theta, \quad \tilde{\mathbf{C}}_{2k,s} = \frac{1}{\pi}\int_0^{2\pi} h_s(\theta)\sin(k\theta)d\theta. \tag{42}$$

Then $\tilde{\mathbf{C}}\mathbf{C} = \mathbf{I}$. *In particular, if* N *is odd, the matrix* $\tilde{\mathbf{C}}$ *can be calculated as*

$$\tilde{\mathbf{C}}_{2k-1,s} = \frac{2}{N}\sum_{n=1}^{N} h_s\left(\frac{2\pi n}{N}\right)\cos\left(\frac{2\pi kn}{N}\right), \quad \tilde{\mathbf{C}}_{2k,s} = \frac{2}{N}\sum_{n=1}^{N} h_s\left(\frac{2\pi n}{N}\right)\sin\left(\frac{2\pi kn}{N}\right). \tag{43}$$

Proof. Given $v = (\alpha_1, \beta_1, \dots, \alpha_K, \beta_K) \in \mathbb{C}^{2K}$, and f the associated function defined by (34), we have $(\mathbf{C}v)_n = f(\theta_n)$ for $n = 1, \dots, N$. Using (39) and (42), we find that

$$(\tilde{\mathbf{C}}\mathbf{C}v)_{2k-1} = \frac{1}{\pi}\int_0^{2\pi} f(\theta)\cos(k\theta)d\theta = \alpha_k, \tag{44}$$

$$(\tilde{\mathbf{C}}\mathbf{C}v)_{2k} = \frac{1}{\pi}\int_0^{2\pi} f(\theta)\sin(k\theta)d\theta = \beta_k, \tag{45}$$

Copyright © by SIAM. Unauthorized reproduction of this article is prohibited.

and, therefore, $\tilde{\mathbf{C}}\mathbf{C}v = v$. Observe that $h_s(\theta)$, $\cos(k\theta)$, and $\sin(k\theta)$ all belong to $V_{\lfloor N/2 \rfloor}$, so when N is odd, we easily deduce (43) using (37). ∎

Remark 4.1. Proposition 4.5 can be used in the noiseless limited-view case to reconstruct the CGPT matrix $\mathbf{M}$ from the MSR measurements $\mathbf{V}$. In fact, from (6) it immediately follows that

$$\mathbf{M} = \mathbf{D}^{-1}\tilde{\mathbf{C}}\mathbf{V}\tilde{\mathbf{C}}^{\top}\mathbf{D}^{-1}.$$

This shows that in the noiseless case, the limited-view aspect has no effect on the reconstruction of the GPTs and consequently on the location and orientation tracking. In the presence of noise, the effect, as will be shown in the next subsection, is dramatic. A small amount of measurement noise significantly changes the performance of our algorithm unless the arrays of receivers and transmitters offer a directional diversity; see Figure 6.

4.3. Ill-posedness in the limited-view setting. We undertake a numerical study to illustrate the ill-posedness of the linear system (7) in the case of limited-view data. Figure 3 shows the distribution of eigenvalues of the matrix $\mathbf{C}^{\top}\mathbf{C}$ and $\mathbf{D}\mathbf{C}^{\top}\mathbf{C}\mathbf{D}$ at different values of γ with $N = 101$ and $K = 50$. In Figure 4, we calculate the condition number of $\mathbf{C}^{\top}\mathbf{C}$ and $\mathbf{L}$ (which is equal to that of $\mathbf{D}\mathbf{C}^{\top}\mathbf{C}\mathbf{D}$ by (32)) for different orders K. From these results, we see clearly the effect of the limited-view aspect. First, the tail of tiny eigenvalues in Figure 3(a) suggests that the matrix $\mathbf{C}^{\top}\mathbf{C}$ is numerically singular, despite the fact that $\mathbf{C}$ is of maximal rank. Second, both $\mathbf{C}^{\top}\mathbf{C}$ and $\mathbf{L}$ rapidly become extremely ill-conditioned as K increases, so the maximum resolving order of CGPTs is very limited. Furthermore, this limit is intrinsic to the angle of view and cannot be improved by increasing the number of sources/receivers; see Figure 4 (c) and (d).

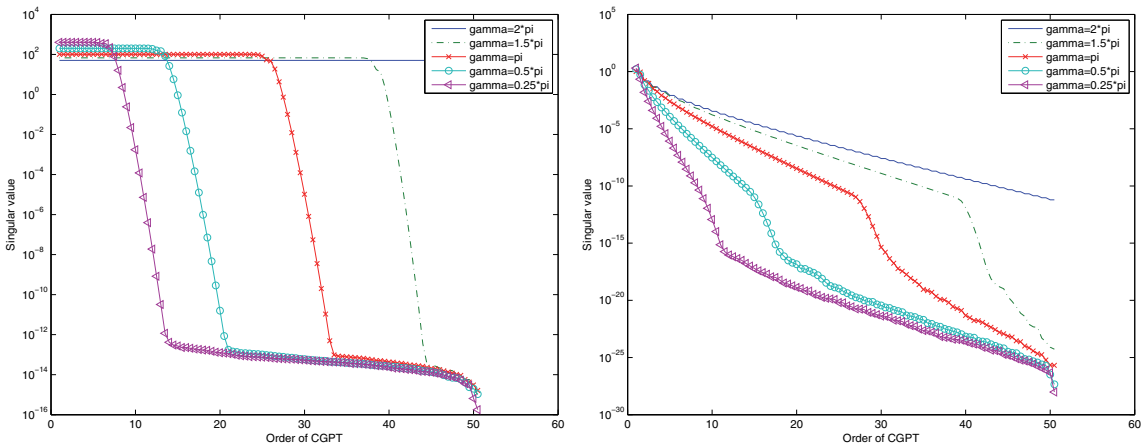

(a) Eigenvalues of $\mathbf{C}^{\top}\mathbf{C}$ (b) Eigenvalues of $\mathbf{D}\mathbf{C}^{\top}\mathbf{C}\mathbf{D}$

Figure 3. *Distribution of eigenvalues (in log scale) of the matrices* $\mathbf{C}^{\top}\mathbf{C}$ (a) *and* $\mathbf{D}\mathbf{C}^{\top}\mathbf{C}\mathbf{D}$ (b). $N = 101$ *sources are equally spaced between* $[0, \gamma)$ *on a circle of radius* $\rho = 1.2$, *and* $K = 50$. *Each curve corresponds to a different value of* γ. *The matrices* $\mathbf{C}^{\top}\mathbf{C}$ *and* $\mathbf{D}\mathbf{C}^{\top}\mathbf{C}\mathbf{D}$ *are calculated from these parameters, and their eigenvalues are sorted in decreasing order.*

Downloaded 08/02/13 to 147.210.110.133. Redistribution subject to SIAM license or copyright; see http://www.siam.org/journals/ojsa.php

Copyright © by SIAM. Unauthorized reproduction of this article is prohibited.

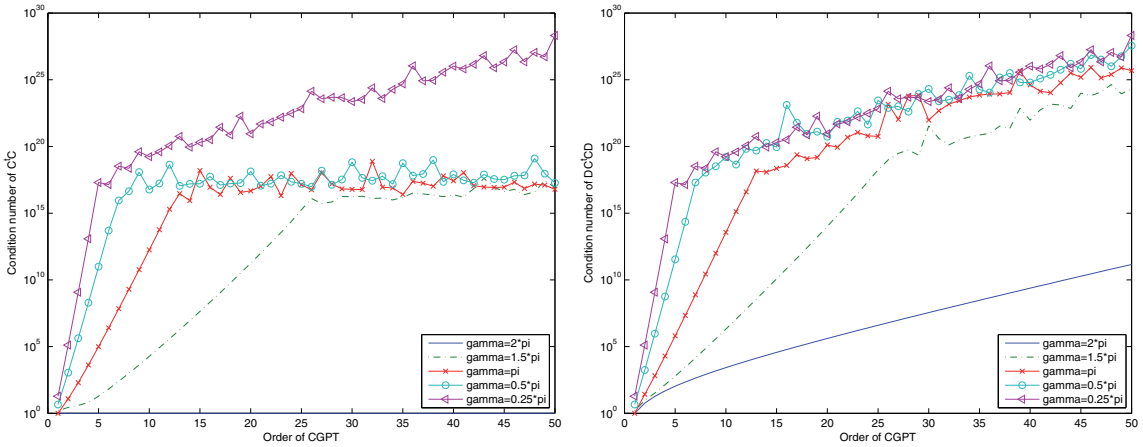

(a) Condition number of $\mathbf{C}^\top\mathbf{C}$ (b) Condition number of $\mathbf{L}$

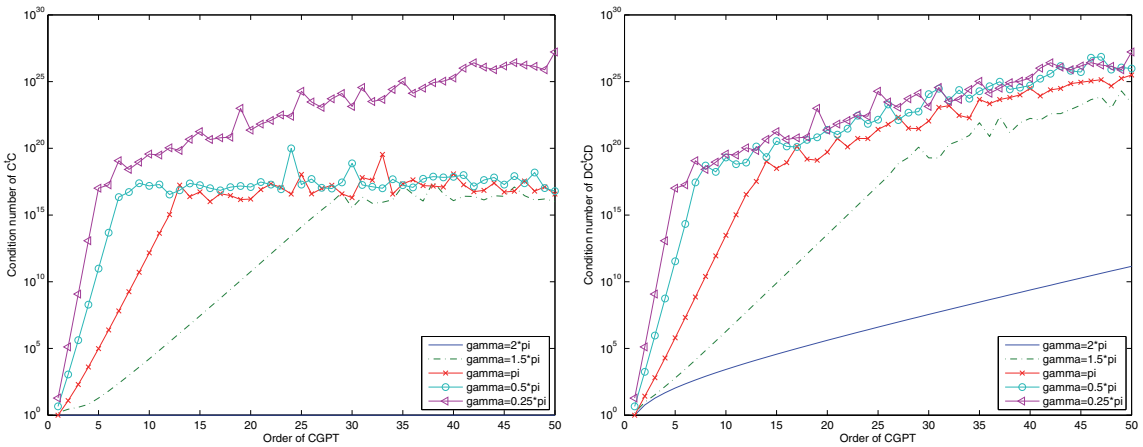

(c) Condition number of $\mathbf{C}^\top\mathbf{C}$ (d) Condition number of $\mathbf{L}$

Figure 4. *Condition numbers (in log scale) of the matrix* $\mathbf{C}^\top\mathbf{C}$ (a) *and the operator* $\mathbf{L}$ (b) *for different orders* K *between* $[1, 50]$. *As in Figure* 3, $N = 101$ *sources are equally spaced between* $[0, \gamma)$ *on a circle of radius* $\rho = 1.2$. (c) *and* (d) *are the same experiment as* (a) *and* (b) *but with* $N = 1001$.

4.4. Reconstruction of CGPTs.

The analysis above suggests that the least-squares problem (8) is not adapted to the CGPT reconstruction in a limited-view setting. Actually, the truncation error or the noise of measurement will be amplified by the tiny singular values of $\mathbf{L}$ and will yield extremely unstable reconstruction of high-order CGPTs, e.g., $K \geq 2$. Instead, in order to reconstruct CGPTs from the MSR data, we can use Tikhonov regularization and solve

$$\min_{\mathbf{M}} \|\mathbf{L}(\mathbf{M}) - \mathbf{V}\|_F^2 + \mu\|\mathbf{M}\|_F^2, \tag{46}$$

with $\mu > 0$ a small regularization constant. It is well known that the effect of the regularization term is to truncate those singular values of $\mathbf{L}$ smaller than μ, which consequently stabilizes the solution. The optimal choice of μ depends on the noise level, and here we determine it from the range $[10^{-6}, 10^{-1}]$ by comparing the solution of (46) with the true CGPTs.

Copyright © by SIAM. Unauthorized reproduction of this article is prohibited.

Downloaded 08/02/13 to 147.210.110.133. Redistribution subject to SIAM license or copyright; see http://www.siam.org/journals/ojsa.php

Here we reconstruct the CGPTs of an ellipse with the parameters $N = 101, K = 50$, and γ varying between 0 and 2π. The major and minor axes of the ellipse are 1 and 0.5, respectively. Figure 5 shows the error of the first two order CGPTs reconstructed through (46) and (8) at three different noise levels. It can be seen that, for small γ, the error obtained by (46) is substantially smaller.

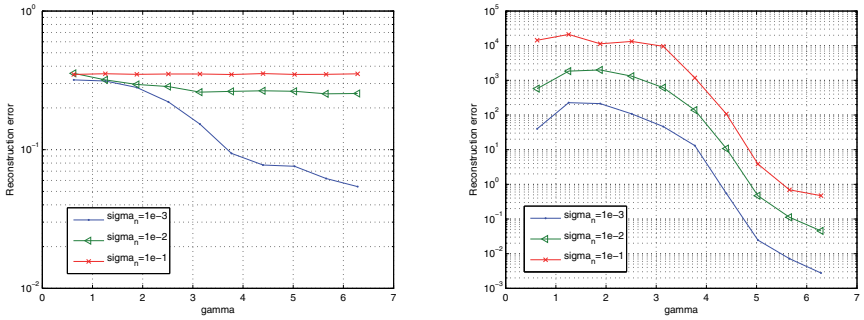

(a) (b)

Figure 5. *Error of reconstructed CGPT of an ellipse compared with true CGPT values at different noise levels. We solve* (46) *and* (8) *with* $N = 101, K = 50$ *and compare the first two orders with the true CGPT. The* x*-axis is the angle of view* γ*.* (a) *Results of* (46)*.* (b) *Results of* (8)*.*

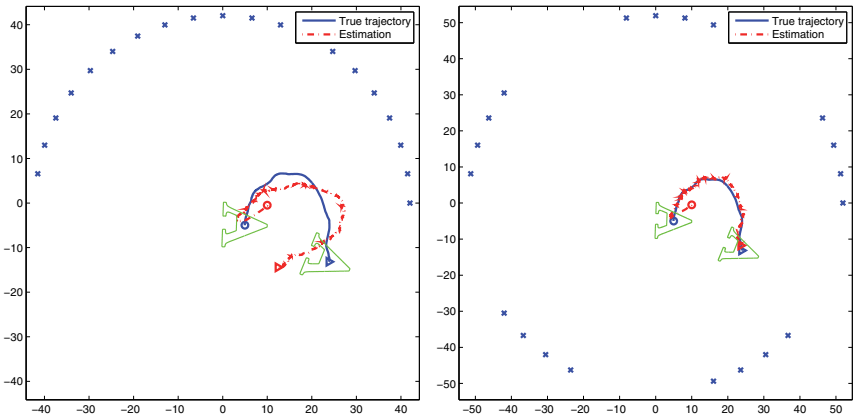

Figure 6. *Same experiment as in Figure* 1*, with a limited angle of view* $\gamma = \pi$*. In* (a) *sources/receivers are equally distributed between* $[0, \gamma)$*, while in* (b) *they are divided into five groups.*

4.5. Tracking in the limited-view setting. The performance of the tracking algorithm can also be affected by the limited angle of view. We repeat the experiment of subsection 3.3 with $\delta = 10$, $\gamma = \pi$, and the same initial guess. In the first configuration, $N = 21$ sources/receivers are equally distributed between $[0, \gamma)$; see Figure 6(a). The results of tracking by the EKF presented in Figures 7 (a), (c), and (e) show large deviations in the estimation of position and a totally wrong estimation of orientation. In the second configuration, we divide the sources/receivers into five groups placed in a nonuniform way on $[0, 2\pi)$, and each group

Copyright © by SIAM. Unauthorized reproduction of this article is prohibited.

Downloaded 08/02/13 to 147.210.110.133. Redistribution subject to SIAM license or copyright; see http://www.siam.org/journals/ojsa.php

covers only an angle range of 0.2π; see Figure 6(b). Although the total angular coverages are the same in both configurations, the second gives much better tracking results, as shown in Figures 7 (b), (d), and (f). These results clearly demonstrate the importance of a large angle of view (or a directional diversity) for the tracking problem.

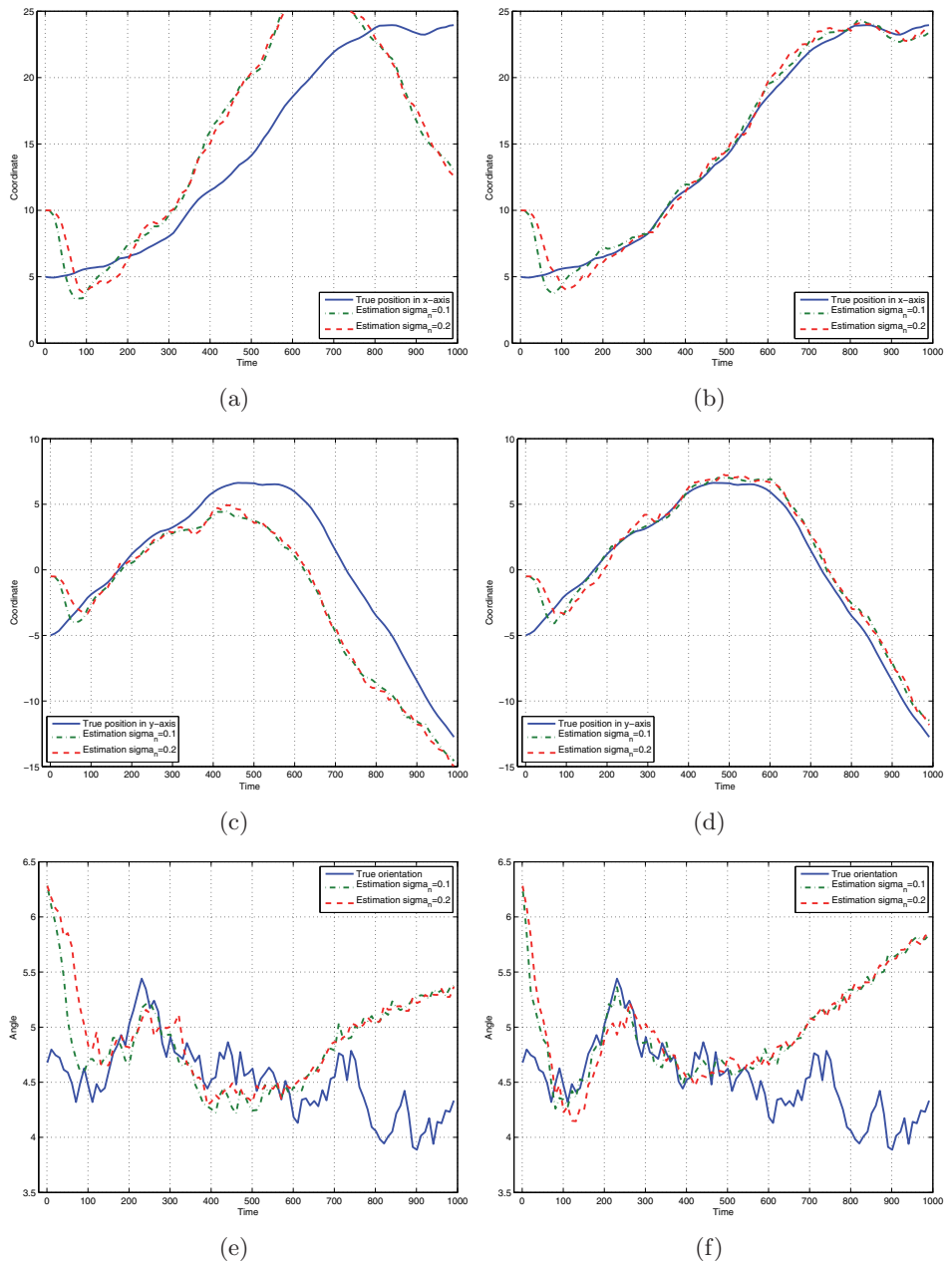

Figure 7. *Results of tracking using the configuration of Figure 6 at different noise levels. First row: Coordinate in x-axis. Second row: Coordinate in y-axis. Last row: Orientation. The first and second columns correspond to the configuration in Figures 6* (a) *and* (b)*, respectively.*

Downloaded 08/02/13 to 147.210.110.133. Redistribution subject to SIAM license or copyright; see http://www.siam.org/journals/ojsa.php

Copyright © by SIAM. Unauthorized reproduction of this article is prohibited.

Downloaded 08/02/13 to 147.210.110.133. Redistribution subject to SIAM license or copyright; see http://www.siam.org/journals/ojsa.php

5. Conclusion. In this paper we have provided a location and orientation tracking of a mobile target from MSR measurements in the full- and limited-view settings. Our algorithm is based on the concept of GPTs. In the limited-view case, the effect of noise on the tracking is severe. However, if the arrays of receivers and transmitters offer a good directional diversity, then satisfactory results can be obtained. It would be interesting to generalize our algorithms for tracking multiple targets. As a first step, a matching pursuit algorithm [23] would be appropriate for recognizing the targets. Establishing Cramer–Rao lower bounds on location and orientation for multiple targets would be also interesting [12]. This will be the subject of a forthcoming work.

Appendix A. Kalman filter. The KF is a recursive method that uses a stream of noisy observations to produce an optimal estimator of the underlying system state [22]. Consider the following time-discrete dynamical system ($t \geq 1$):

$$X_t = F_t X_{t-1} + W_t, \tag{47}$$

$$Y_t = H_t X_t + V_t, \tag{48}$$

where the following hold:

- X_t is the vector of *system state*.
- Y_t is the vector of *observation*.
- F_t is the state transition matrix which is applied to the previous state X_{t-1}.
- H_t is the observation matrix which yields the (noise-free) observation from a system state X_t.
- $W_t \sim \mathcal{N}(0, Q_t)$ is the process noise and $V_t \sim \mathcal{N}(0, R_t)$ is the observation noise, with, respectively, Q_t and R_t the covariance matrices. These two noises are independent of one another. Further, we assume that, for $t \neq \tau$, W_t and W_τ are also independent (the same holds for V_t and V_τ).

Suppose that X_0 is Gaussian. Then it follows that the process $(X_t, Y_t)_{t\geq 0}$ is Gaussian. The objective is to estimate the system state X_t from the accumulated observations $Y_{1:t} := [Y_1 \dots Y_t]$.

The optimal estimator (in the least-squares sense) of the system state X_t given the observations $Y_{1:t}$ is the conditional expectation

$$\hat{x}_{t|t} = \mathbb{E}[X_t | Y_{1:t}]. \tag{49}$$

Since the joint vector $(X_t, Y_{1:t})$ is Gaussian, the conditional expectation $\hat{x}_{t|t}$ is a linear combination of $Y_{1:t}$, which can be written in terms of $\hat{x}_{t-1|t-1}$ and Y_t only. The purpose of the KF is to calculate $\hat{x}_{t|t}$ from $\hat{x}_{t-1|t-1}$ and Y_t.

We summarize the algorithm in the following.

Initialization:

$$\hat{x}_{0|0} = \mathbb{E}[X_0], \;\; P_{0|0} = \operatorname{cov}(X_0). \tag{50}$$

Prediction:

$$\hat{x}_{t|t-1} = F_t \hat{x}_{t-1|t-1}, \tag{51}$$

$$\tilde{Y}_t = Y_t - H_t \hat{x}_{t|t-1}, \tag{52}$$

$$P_{t|t-1} = F_t P_{t-1|t-1} F_t^T + Q_t. \tag{53}$$

Copyright © by SIAM. Unauthorized reproduction of this article is prohibited.

Update:

$$S_t = H_t P_{t|t-1} H_t^T + R_t, \tag{54}$$

$$K_t = P_{t|t-1} H_t^T S_t^{-1}, \tag{55}$$

$$\hat{x}_{t|t} = \hat{x}_{t|t-1} + K_t \tilde{Y}_t, \tag{56}$$

$$P_{t|t} = (I - K_t H_t) P_{t-1|t-1}. \tag{57}$$

To apply the KF algorithm the covariance matrices Q_t, R_t must be known.

Appendix B. Extended Kalman filter. Consider now a nonlinear dynamical system

$$X_t = f_t(X_{t-1}, W_t), \tag{58}$$

$$Y_t = h_t(X_t, V_t), \tag{59}$$

where X_t, Y_t, W_t, V_t are the same as in the KF, while the functions f_t, h_t are nonlinear and differentiable. Nothing can be said in general about the conditional distribution $X_t|Y_{1:t}$ due to the nonlinearity. The EKF calculates an approximation of the conditional expectation (49) by an appropriate linearization of the state transition and observation models, which makes the general scheme of the KF still applicable [28]. However, the resulting algorithm is no more optimal in the least-squares sense due to the approximation.

Let $F_X = \partial_X f(\hat{x}_{t-1|t-1}, 0), F_W = \partial_W f(\hat{x}_{t-1|t-1}, 0)$, the partial derivatives of f (with respect to the system state and the process noise) be evaluated at $(\hat{x}_{t-1|t-1}, 0)$, and $H_X = \partial_X h(\hat{x}_{t|t-1}, 0), H_V = \partial_V h(\hat{x}_{t|t-1}, 0)$ be the partial derivatives of h (with respect to the system state and the observation noise) evaluated at $(\hat{x}_{t|t-1}, 0)$. The EKF algorithm is summarized below.

Initialization:

$$\hat{x}_{0|0} = \mathbb{E}[X_0], \ P_{0|0} = \mathrm{cov}(X_0). \tag{60}$$

Prediction:

$$\hat{x}_{t|t-1} = f(\hat{x}_{t-1|t-1}, 0), \tag{61}$$

$$\tilde{Y}_t = Y_t - h(\hat{x}_{t|t-1}, 0), \tag{62}$$

$$P_{t|t-1} = F_X P_{t-1|t-1} F_X^T + F_W Q_t F_W^T. \tag{63}$$

Update:

$$S_t = H_X P_{t|t-1} H_X^T + H_V R_t H_V^T, \tag{64}$$

$$K_t = P_{t|t-1} H_X^T S_t^{-1}, \tag{65}$$

$$\hat{x}_{t|t} = \hat{x}_{t|t-1} + K_t \tilde{Y}_t, \tag{66}$$

$$P_{t|t} = (I - K_t H_X) P_{t-1|t-1}. \tag{67}$$

Downloaded 08/02/13 to 147.210.110.133. Redistribution subject to SIAM license or copyright; see http://www.siam.org/journals/ojsa.php

Copyright © by SIAM. Unauthorized reproduction of this article is prohibited.

REFERENCES

[1] H. Ammari, T. Boulier, and J. Garnier, *Modeling active electrolocation in weakly electric fish*, SIAM J. Imaging Sci., 6 (2013), pp. 285–321.

[2] H. Ammari, T. Boulier, J. Garnier, W. Jing, H. Kang, and H. Wang, *Target identification using dictionary matching of generalized polarization tensors*, preprint, arXiv:1204.3035, 2012; Found. Comput. Math., to appear.

[3] H. Ammari, T. Boulier, J. Garnier, and H. Wang, *Shape identification and classification in electrolocation*, preprint, arXiv:1302.6384, 2013.

[4] H. Ammari, J. Garnier, H. Kang, M. Lim, and S. Yu, *Generalized polarization tensors for shape description*, Numer. Math., to appear. DOI 10.1007/s00211-013-0561-5.

[5] H. Ammari and H. Kang, *Reconstruction of Small Inhomogeneities from Boundary Measurements*, Lecture Notes in Math. 1846, Springer-Verlag, Berlin, 2004.

[6] H. Ammari and H. Kang, *Polarization and Moment Tensors: With Applications to Inverse Problems and Effective Medium Theory*, Appl. Math. Sci. 162, Springer-Verlag, New York, 2007.

[7] H. Ammari and H. Kang, *High-order terms in the asymptotic expansions of the steady-state voltage potentials in the presence of conductivity inhomogeneities of small diameter*, SIAM J. Math. Anal., 34 (2003), pp. 1152–1166.

[8] H. Ammari and H. Kang, *Properties of generalized polarization tensors*, Multiscale Model. Simul., 1 (2003), pp. 335–348.

[9] H. Ammari, H. Kang, M. Lim, and H. Lee, *Enhancement of near cloaking using generalized polarization tensors vanishing structures. Part I: The conductivity problem*, Comm. Math. Phys., 317 (2013), pp. 253–266.

[10] H. Ammari, H. Kang, M. Lim, and H. Zribi, *The generalized polarization tensors for resolved imaging. Part I: Shape reconstruction of a conductivity inclusion*, Math. Comp., 81 (2012), pp. 367–386.

[11] H. Ammari, H. Kang, and K. Touibi, *Boundary layer techniques for deriving the effective properties of composite materials*, Asymptot. Anal., 41 (2005), pp. 119–140.

[12] Y. Bar-Shalom and X. Li, *Estimation and Tracking: Principles, Techniques, and Software*, Artech House, Boston, MA, 1993.

[13] Y. Capdeboscq, A. B. Karrman, and J.-C. Nédélec, *Numerical computation of approximate generalized polarization tensors*, Appl. Anal., 91 (2012), pp. 1189–1203.

[14] D. J. Cedio-Fengya, S. Moskow, and M. S. Vogelius, *Identification of conductivity imperfections of small diameter by boundary measurements: Continuous dependence and computational reconstruction*, Inverse Problems, 14 (1998), pp. 553–595.

[15] M. Cheney and B. Borden, *Imaging moving targets from scattered waves*, Inverse Problems, 24 (2008), 035005.

[16] D. Clark, I. T. Ruiz, Y. Petillot, and J. Bell, *Particle PHD filter multiple target tracking in sonar images*, IEEE Trans. Aerospace Electr. Syst., 43 (2007), pp. 409–416.

[17] G. Dassios and R. Kleinman, *Low Frequency Scattering*, Oxford Math. Monogr., Oxford University Press, New York, 2000.

[18] D. Daviesy, P. Palmery, and M. Mirmehdi, *Detection and tracking of very small low contrast objects*, in Proceedings of the British Machine Vision Conference, Southampton, UK, 1998, pp. 599–608.

[19] A. Friedman and M.S. Vogelius, *Identification of small inhomogeneities of extreme conductivity by boundary measurements: A theorem on continuous dependence*, Arch. Ration. Mech. Anal., 105 (1989), pp. 299–326.

[20] C. D. Haworth, Y. De Saint-Pern, D. Clark, E. Trucco, and Y. R. Petillot, *Detection and tracking of multiple metallic objects in millimetre-wave images*, Internat. J. Comput. Vision, 71 (2007), pp. 183–196.

[21] J. S. Jaffe, *Target localization for a three-dimensional multibeam sonar imaging system*, J. Acoust. Soc. Amer., 105 (1999), pp. 3168–3175.

[22] R. E. Kalman, *A new approach to linear filtering and prediction problems*, Trans. ASME J. Basic Engrg., 82 (1960), pp. 35–45.

[23] S. Mallat, *A Wavelet Tour of Signal Processing*, Academic Press, San Diego, CA, 1998.

Downloaded 08/02/13 to 147.210.110.133. Redistribution subject to SIAM license or copyright; see http://www.siam.org/journals/ojsa.php

Copyright © by SIAM. Unauthorized reproduction of this article is prohibited.

[24] E. Margolis and Y. C. Eldar, *Nonuniform sampling of periodic bandlimited signals*, IEEE Trans. Signal Process., 56 (2008), pp. 2728–2745.
[25] G. W. Milton, *The Theory of Composites*, Cambridge Monogr. Appl. Comput. Math., Cambridge University Press, Cambridge, UK, 2001.
[26] G. Pólya and G. Szegö, *Isoperimetric Inequalities in Mathematical Physics*, Ann. of Math. Stud. 27, Princeton University Press, Princeton, NJ, 1951.
[27] L. Wang, M. Cheney, and B. Borden, *Multistatic radar imaging of moving targets*, in Proceedings of the IEEE Radar Conference, IEEE, Washington, DC, 2010, pp. 391–396.
[28] G. Welch and G. Bishop, *An introduction to the Kalman filter*, in Proceedings of SIGGRAPH 2001 (Los Angeles, CA), ACM, New York, 2001.
[29] A. Zygmund, *Trigonometric Series*, Cambridge University Press, Cambridge, UK, 1988.

Downloaded 08/02/13 to 147.210.110.133. Redistribution subject to SIAM license or copyright; see http://www.siam.org/journals/ojsa.php

Copyright © by SIAM. Unauthorized reproduction of this article is prohibited.